



Contents lists available at ScienceDirect

International Journal for Parasitology: Drugs and Drug Resistance

journal homepage: www.elsevier.com/locate/ijpddr

Untargeted metabolomic analysis of miltefosine action in *Leishmania infantum* reveals changes to the internal lipid metabolism [☆]

Isabel M. Vincent ^a, Stefan Weidt ^b, Luis Rivas ^c, Karl Burgess ^b, Terry K. Smith ^d, Marc Ouellette ^{a,*}^a Centre de Recherche en Infectiologie, Université Laval, Québec, Canada^b Glasgow Polyomics Facility, University of Glasgow, Glasgow, UK^c Centro de Investigaciones Biológicas (CSIC), Madrid, Spain^d Schools of Biology & Chemistry, Biomedical Sciences Research Complex (BSRC), The North Haugh, The University, St. Andrews, UK

ARTICLE INFO

Article history:

Received 6 September 2013

Received in revised form 8 November 2013

Accepted 14 November 2013

Available online 5 December 2013

Keywords:

Miltefosine

Leishmania

Metabolomics

Mode of action

ABSTRACT

There are many theories as to the mode of action of miltefosine against *Leishmania* including alterations to the membrane lipid content, induction of apoptosis and modulation of macrophage responses. Here we perform untargeted metabolomics to elucidate the metabolic changes involved in miltefosine action. Over 800 metabolites were detected, 10% of which were significantly altered after 3.75 h. Many of the changes related to an increase in alkane fragment and sugar release. Fragment release is synchronised with reactive oxygen species production, but native membrane phospholipids remain intact. Signs of DNA damage were also detected as were changes to the levels of some thiols and polyamines. After 5 h of miltefosine treatment the cells showed depleted levels of most metabolites, indicating that the cells' outer membrane integrity had become compromised and internal metabolites were escaping upon cell death. In miltefosine resistant cells, the drug was not internalised and the changes to the internal metabolite levels were not seen. In contrast, cells resistant to antimony (SbIII) had similar corresponding alterations to the levels of internal metabolites as wild-type cells. A detailed knowledge of the mode of action of miltefosine will be important to inform the design of combination therapies to combat leishmaniasis, something that the research community should be prioritising in the coming years.

© 2013 The Authors. Published by Elsevier Ltd. All rights reserved.

1. Introduction

The species of the *Leishmania* genus of protozoan parasites are responsible for significant morbidity and mortality in 88 countries in Africa, the Middle East, Asia, Southern Europe and South and Central America (WHO, 2010). Treatments for the complex of diseases caused by *Leishmania* vary depending on the infective species and the geographical location of infection. The compounds range between the ancient and toxic antimonial therapies to the newer, more targeted amphotericin B liposomal formulations (Croft et al., 2006). The alkylphosphocholine drug miltefosine, is the first and only orally-available leishmanicide, available after having first being developed as an antineoplastic agent. It has been licensed for 10 years in India for the treatment of visceral leishmaniasis and can also be used to treat cutaneous disease (Dorlo et al., 2012).

Resistance in the field has not yet been reported, but it is readily selected for in the laboratory (Pérez-Victoria et al., 2006a; Seiferta et al., 2007; Choudhury et al., 2008; Coelho et al., 2012), and higher drug concentrations may start to be required to prevent parasite recrudescence in the field.

The mechanism of action (MOA) of miltefosine has been the subject of some debate, which may indicate the presence of multiple targets, or may be due to the different experimental designs and analyses carried out. Traditionally, miltefosine has been considered as an inhibitor of protein kinase B (Akt or PKB) in humans, which is part of a signalling pathway involved in the induction of apoptosis (Ruiter et al., 2003). Similar pathways have not been seen in *Leishmania*, however, nor has binding of miltefosine to a *Leishmania* analogue of Akt. Other theories for the miltefosine MOA in *Leishmania* include: alterations to the membrane lipid content and modulation of macrophage responses, although clearly the latter would not be involved in insect stage (promastigote) responses to the drug.

Lux et al. (1996) suggested that ether lipid metabolism, GPI anchor biosynthesis and signal transduction were putative targets of miltefosine. Further studies analysed the effects of miltefosine on prepared lipid monolayers indicating interactions leading miltefosine to be inserted into the monolayers (Rakotomanga

[☆] This is an open-access article distributed under the terms of the Creative Commons Attribution-NonCommercial-No Derivative Works License, which permits non-commercial use, distribution, and reproduction in any medium, provided the original author and source are credited.

* Corresponding author. Address: Centre de Recherche en Infectiologie du CHUL, 2705, boul. Laurier, Québec G1V 4G2, Canada. Tel.: +1 (418) 654 2705; fax: +1 (418) 654 2715.

E-mail address: Marc.Ouellette@crchu.ulaval.ca (M. Ouellette).

et al., 2004). Miltefosine also affects the cell membrane of *in situ* promastigotes leading to an increased phosphatidylethanolamine and lysophosphatidylcholine content (Rakotomanga et al., 2007). A more recent analysis of membrane phospholipids by liquid chromatography mass spectrometry provided a more detailed analysis of the lipid species altered after miltefosine administration and revealed a more complicated picture with different classes of lipids showing changes to some, but not all group members (Imbert et al., 2012). Miltefosine has also been shown to interfere with choline transport (Zufferey and Mamoun, 2002), which may account for some of the changes to the phospholipid content of the membrane.

The apoptosis theory of miltefosine MOA was conceived after the observation of some of the classical signs of apoptosis such as an increase in reactive oxygen species, nuclear condensation, DNA fragmentation and a loss of membrane potential (Moreira et al., 2011). These signs, however, could also be due to non-regulated cell death, which was recently reviewed (Proto et al., 2013).

Resistance to miltefosine in *Leishmania* points to a transporter defect, with two transporters implicated (miltefosine transporter (MT)) coupled to its regulatory subunit ROS3 (Pérez-Victoria et al., 2006b) for inward translocation and an ABC transporter to expel the drug (Pérez-Victoria et al., 2006a). The fact that the drug is internalised means that it would be particularly useful to study changes to the internal metabolite repertoire after the administration of miltefosine. The alterations to the membrane lipid complement may then be explained by an internal metabolic or catabolic mechanism and this should not happen in resistant cells, in which miltefosine is not translocatable.

We present here our comparison of the internal metabolite repertoire between wild-type promastigotes treated with miltefosine and two resistant lines: a miltefosine resistant line, in which we do not expect to see metabolic changes and an antimony (SbIII) resistant line, to ensure the specificity of changes observed.

2. Materials and methods

2.1. Culture and resistance selection

The *Leishmania infantum* JPCM5 promastigote cell line was used as the wild-type parent line from which the derived lines MF200 and SbIII2000.2 were selected by a stepwise increase in drug pressure and were resistant to 200 μ M miltefosine (Cayman Chemical, Ann Harbor, USA) or 2 mM SbIII (Potassium antimonyl tartrate trihydrate, Aldrich, USA) respectively. The wild-type IC_{50} s for miltefosine and SbIII are 15 μ M and 70 μ M respectively (data not shown). Cells were not clonal and grew at a rate similar to wild-type. Cells were maintained in medium 199 (M199; Gibco) supplemented with 10% heat-inactivated foetal bovine serum and 10 μ g/ml haemin at 28 °C and either 200 μ M of miltefosine or 2 mM SbIII.

IC_{90} s were taken by serial dilution of drug in 96 well transparent plates before addition of cells at a final concentration of 2.5×10^6 /ml and incubation at 28 °C with shaking for 72 h. The optical density of each well in the plate was read at a wavelength of 600 nm and analysed using Graphpad Prism5 using non-linear regression analysis.

2.2. Metabolomics

Cells were inoculated at 5×10^6 /ml in M199 from a log-phase culture and miltefosine was added at 20.6 μ M (IC_{90}). Samples were taken at the time taken for 50% of wild-type cells to die (5 h) as well as time points (0, 1.25, 2.5 and 3.75 h) up to 5 h. All samples were taken in triplicate from independent cultures. Cell metabolism in 4×10^7 cells was quenched by rapid cooling to 4 °C in a

dry ice-ethanol bath before centrifugation at 1250g for 5 min to remove medium. Residual medium was removed by washing in 4 °C HEPES–NaCl and cells were lysed and proteins precipitated by shaking in 200 μ L 4 °C chloroform:methanol:water (1:3:1) plus standards (theophylline, 5-fluorouridine, N-methyl glucamine, canavanine and piperazine, all at 1 μ M) for 1 h. Protein precipitate was removed by centrifugation and a 10 μ L aliquot of the supernatant was injected onto a 150 mm \times 4.6 mm 5 μ m 200 Å ZIC–HILIC HPLC column (SeaQuant, Merck). The column was coupled to an Orbitrap Exactive (Thermo) and masses and retention times were detected using a previously published method (Vincent et al., 2012). Data analysis was performed using mzMatch (Scheltema et al., 2011) and Excel (Microsoft) with a VBS macro-based package called IDEOM (Creek et al., 2012) for further filtering and metabolite annotation. The independent biological replicates were taken for each time point from separate cultures on different days. These were run on the mass spectrometer in the same run.

Five internal standards were used to correct for mass drift and a further mixture of 143 standards was used to create the retention time calculator in IDEOM, allowing accurate mass and retention time identification as well as metabolite validation. Masses were filtered through mzMatch keeping those that were reproducible across all three biological replicates at each time point, had relative standard deviations below 0.5 and had intensities above 3000. Metabolites were further filtered in IDEOM (version 13) to have a retention time error of below 35% and mass errors below three parts per million (ppm) for those metabolites with predicted retention times of below 5% and three ppm for metabolites with a standard. Partial least squares analysis was performed using Metaboanalyst after pre-processing in IDEOM and data filtering using the relative standard deviation (<http://www.metaboanalyst.ca/>).

2.3. Miltefosine uptake

Log phase cells were washed in HEPES–NaCl and re-suspended to 4×10^8 /ml. 100 μ L of the cell suspension was added to 100 μ L of 5 μ M MT-11C-BODIPY (11-(4',4'-Difluoro-1',3',5',7'-tetramethyl-4'-bora-3'a,4'a-diaza-s-indacen-2'-yl) undecyl-phosphocholine) (Hornillos et al., 2008) in HEPES–NaCl and tubes were left in the dark at room temperature for varying lengths of time before washing twice in 1 ml HEPES–NaCl. Cells were re-suspended to 200 μ L in HEPES–NaCl and the fluorescence was read (Victor2, Perkin Elmer, Turku, Finland) at excitation 485 nm, emission 535 nm for 1 s per well. The fluorescence of 5 μ M MT-11C-BODIPY was also read and this figure was used to calculate the moles of internalised miltefosine. At least three biological replicates were taken for each time point.

2.4. ROS measurements

4×10^7 cells were taken from a log phase culture at 5×10^6 cells/ml at time points 0, 1.25, 2.5, 3.75 and 5 h after 20.6 μ M miltefosine addition, 5 h being the point at which 50% of wild-type cells are dead compared to untreated cells. Cells were washed twice in 1 mL HEPES–NaCl then re-suspended in 500 μ L HEPES–NaCl containing 40 nM DCFDA (Dichlorofluorescein diacetate, a dye that measures total ROS in live cells) (Invitrogen, Burlington, Ontario, Canada). Cells were left in the dark for 30 min before being washed twice in HEPES–NaCl, and re-suspended in 500 μ L. 200 μ L of the cell suspension was read with a Victor2 fluorometer (Perkin Elmer, Turku) at 485 nm excitation and 535 nm emission. Three independent biological replicates were taken for each time point.

2.5. Sequencing

PCR products of the miltefosine transporter amplified with the primers MT_F 5'/ATGCCCAACCAACCG3' and MT_R 5'/TCACAGCTTTC-CACC3' were ligated to pGEM-T easy (Promega) and sequenced using an in-house platform.

2.6. Microscopy

Cells were fixed in methanol and Giemsa stained using Diff-Quik (Baxter) reagents. The microscope (Nikon Eclipse TE300) was used at 100× magnification using oil immersion. Image Pro (Media Cybernetics) was used to prepare the images.

2.7. Lipid analysis

Total lipids were extracted using a modified Bligh and Dyer method (Bligh and Dyer, 1959). Briefly, cells were washed with PBS, suspended in 100 µl PBS and transferred to a glass tube, 375 µL of 1:2 (v/v) chloroform:methanol were added and vortexed. The sample was agitated vigorously for a further 10–15 min. The sample was made biphasic by the addition of 125 µL chloroform, followed by vortexing and subsequently the addition of 125 µL of H₂O. The mixture was then vortexed again and centrifuged at 1000g at room temperature for 5 min. The lower phase was transferred to a new glass vial and dried under nitrogen and stored in the fridge.

Total lipid extracts were dissolved in 15 µL of 1:2 (v/v) chloroform:methanol and 15 µL of acetonitrile:iso-propanol:water (6:7:2) and analysed with a Absceix 4000 QTrap, a triple quadrupole mass spectrometer equipped with a nanoelectrospray source.

Samples were delivered using a Nanomate interface in direct infusion mode (~125 nl/min). The lipid extracts were analysed in both positive and negative ion modes using a capillary voltage of 1.25 kV. MS/MS scanning (daughter, precursor and neutral loss scans) were performed using nitrogen as the collision gas with collision energies between 35 and 90 V. Each spectrum encompasses at least 50 repetitive scans.

Tandem mass spectra (MS/MS) were obtained with collision energies as follows: 35–45 V, PC/SM in positive ion mode, parent-ion scanning of *m/z* 184; 35–55 V, PI/IPC in negative ion mode, parent-ion scanning of *m/z* 241; 35–65 V, PE in negative ion mode, parent-ion scanning of *m/z* 196; 20–35 V, PS in negative ion mode, neutral loss scanning of *m/z* 87; and 40–90 V, for all glycerophospholipids (including PA, PG and cardiolipin) detected by precursor scanning for *m/z* 153 in negative ion mode. MS/MS daughter ion scanning was performed with collision energies between 35 and 90 V. Assignment of phospholipid species is based upon a combination of survey, daughter, precursor and neutral loss scans, as well previous assignments (Richmond et al., 2010; Williams et al., 2012). The identity of phospholipid peaks was verified using the LIPID MAPS: Nature Lipidomics Gateway (www.lipidmaps.org).

2.8. Thin layer chromatography

2×10^8 log-phase promastigotes were washed in HEPES–NaCl and resuspended at 4×10^8 /ml in HEPES–NaCl. BODIPY–miltefosine was added to a final concentration of 10.4 µM and these samples were incubated for 5 h in the dark at room temperature. Samples were washed and neutral lipids were extracted by resuspending in 1 mL 1:0.5:0.4 methanol:chloroform:water. These were incubated for 1 h, with regular vortexing before centrifuging for 20 min at 3000 RPM. The supernatant was taken and 1 mL 1:0.5:0.4 methanol:chloroform:water was added to the pellet, this was extracted again for 1 h at room temperature with regular

vortexing then centrifuged again. The supernatants were pooled and 1:1 chloroform:water was added until the solution became biphasic. The samples were centrifuged for 30 min at 3000 RPM and the organic phase was taken and evaporated under nitrogen. Lipids were dissolved in 50 µL methanol and spotted onto TLC silica gel 60 F254 paper (Merck). Extracts were run in 15:13:12:40:8 acetone:methanol:acetic acid:chloroform:water for approximately 2 h and read under UV light.

3. Results

3.1. Metabolomics analyses and detection of miltefosine

To ensure that metabolomics samples were collected at biologically relevant drug concentrations and time points, the IC₉₀ of miltefosine was calculated on our wild-type cell line of *L. infantum* JPCM5 over 72 h (Fig. 1a). The IC₉₀ at 72 h (20.6 µM) was then used to determine the time taken for cells to become 50% inhibited according to their cell number compared to untreated cells (Fig. 1b). This was taken as the end point of our experiment with time points taken up to this point. There was significant resistance ($p = 0.001$ from ANOVA with Dunnett's post hoc test) in the miltefosine resistant line, MF200 (miltefosine IC₉₀: 239 µM) and a small, but not significant resistance in the SbIII resistant line, SbIII2000.2 (miltefosine IC₉₀: 37 µM) (Fig. 1a). *Leishmania* cells treated with miltefosine produce reactive oxygen species (ROS) (Moreira et al., 2011; Getachew and Gedamu, 2012). To discriminate between miltefosine-induced and ROS-induced metabolite changes, we tested for ROS production during miltefosine treatment. A gradual miltefosine-induced ROS production was observed in wild-type cells, but not in the MF200 line (Fig. 1c). The SbIII resistant line produced slightly less ROS (Fig. 1c) when challenged with miltefosine, although this was not significantly different to the wild-type miltefosine-induced ROS level.

After processing through mzMatch and IDEOM, 876 feature annotations (assigned to putative metabolites) were identified in the metabolite extracts (Supplementary Table 1). Partial least squares analysis reveals that 81.1% of the separation between the samples groups is in the first and second components (Supplementary Fig. 1). The 143 internal standards enabled 16% of the metabolome to be validated and an accurate prediction based on mass and retention time for the other metabolites (noted as putative). A confidence level for each identification is provided in Supplementary Table 1, and confidence levels below five were excluded from further analyses.

The monoisotopic mass of miltefosine is 407.3164 (based on the empirical formula) and since it is zwitterionic it should be easily detectable in both positive and negative ionisation modes, however the metabolite was not in IDEOM's internal database and therefore not automatically identified. Upon searching the raw data for the mass of miltefosine, it was observed that the miltefosine was internalised in the wild-type cell line, but to a much lesser extent in the MF200 resistant cell line (Fig. 2a). The wild-type line also showed a significant decrease in miltefosine accumulation at the final time point. This correlates with a decrease of the majority of metabolites at this time point, as discussed later. Surprisingly, there was less miltefosine accumulation in the SbIII2000.2 line, as determined by LC–MS at 2.5 and 3.75 h (Fig. 2a), although this difference was not significant ($p > 0.05$ in a Student's *t*-test). As LC–MS metabolomics analyses are semi-quantitative, we chose to verify these miltefosine accumulation results using a fluorescent miltefosine derivative (MT-11C-BODIPY) (Hornillos et al., 2008). While this fluorescent analogue was transported into the wild-type cells, the same reduced uptake phenomenon was seen in the miltefosine resistant cell line (Fig. 2b). A 2.2-fold difference in the amount of

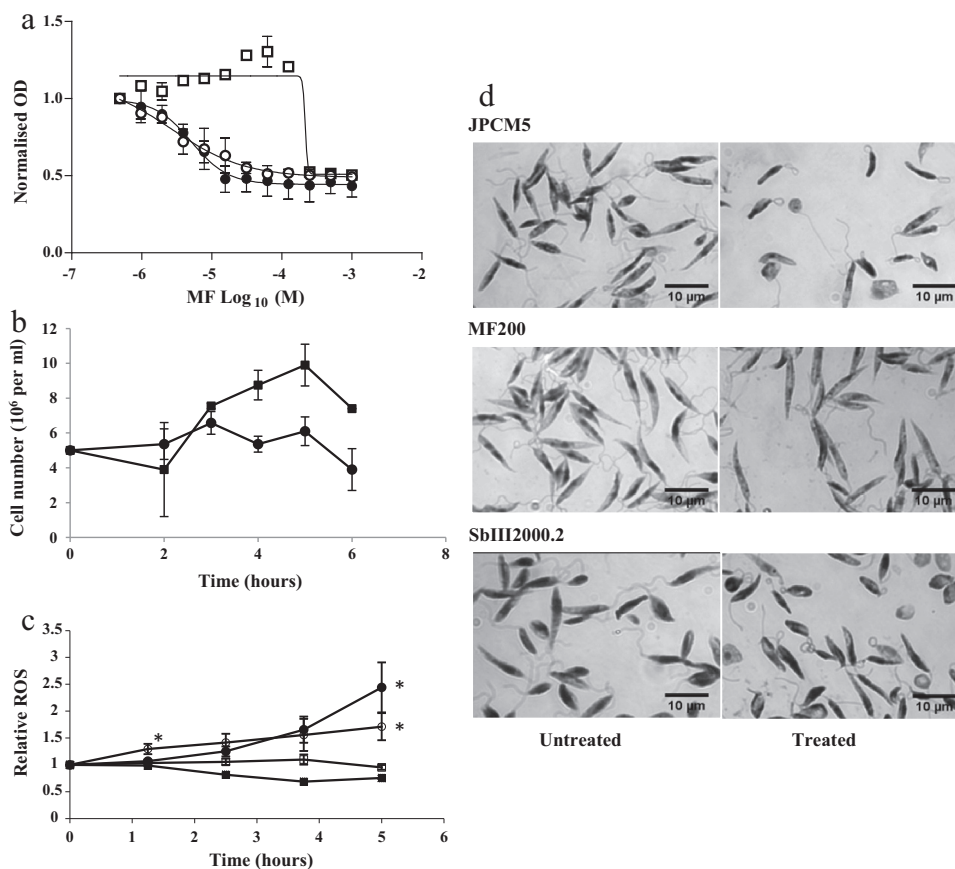


Fig. 1. Miltefosine effects on cell growth, morphology and reactive oxygen species production. (a) The IC₅₀ of miltefosine was measured in JPCM5 (20.6 μM), MF200 (239 μM) and SbIII2000.2 (37.3 μM) cell lines over 72 h. An average of at least three independent biological replicates is shown, with error bars depicting the standard error of the mean. (b) Cell counts during miltefosine treatment at the IC₅₀ in JPCM5 cells show reduced growth by 50% after 5 h. One representative biological replicate (with internal technical replicates) is shown. (c) Relative reactive oxygen species (ROS) production was lower in all resistant lines compared to JPCM5 cells. *Denotes a *p* value of <0.05. An average of at least three independent biological replicates is shown, with error bars depicting the standard error of the mean. (d) Microscopy images of cellular changes after 5 h of miltefosine treatment at IC₅₀. JPCM5 wild-type (●), MF200 (□), SbIII2000.2 (○), and untreated wild-type (■).

miltefosine internalised for SbIII2000.2 over 1 h compared to wild-type JPCM5 was also observed (Fig. 2b) and this was statistically significant ($p < 0.05$ in a Student's *t*-test) at 45 min and 1 h. Miltefosine transport into *Leishmania* is known to involve a transporter complex of the miltefosine transporter (MT, LinJ.13.1590) and ROS3 (LinJ.32.1040) (Pérez-Victoria et al., 2003a,b, 2006b). The MT is frequently mutated in miltefosine resistance, although the mutations seen have been very variable (Coelho et al., 2012). We cloned and sequenced the MT gene from the wild-type and the MF200 and SbIII2000.2 resistant lines. We found no SNP in the wild-type gene, but found a G to A transition in the MT gene of MF200, leading to a G821D amino acid change. This mutation is not in a transmembrane domain or in the ATPase domain. Surprisingly, there were also two mutations in the SbIII2000.2 MT (G26A in the DNA sequence leading to an R9H in the amino acid sequence and C222T which is silent at the amino acid level), which may account for the reduced levels of uptake seen.

The uptake of miltefosine in the wild-type cell line is relatively rapid, with significant uptake seen after 1 h. Since there is not much ROS production at this time point (Fig. 1c), the initial target of miltefosine should be indicated by the metabolite profile at the first time point at 1.25 h in the wild-type cells. There are 60 metabolites with altered levels at this time point in the wild-type cell line, 28 in the resistant line and just three in the SbIII resistant line (Supplementary Table 2). In the wild-type cell line, a metabolite putatively identified as ovoidiol A disulphide is the metabolite that shows the largest reduction in levels between the two time points,

decreasing to 6.9% of the levels in untreated cells after 1.25 h (Supplementary Table 2). This suggests that the thiol is being reduced in preparation for the larger burst of oxidative stress to come. Other metabolites showing altered levels in these cells included a wide range of metabolites putatively identified as hormones, sugars, acids and lipids. One lipid in particular (with a mass of 453.3219) was increased 1629 fold upon miltefosine introduction. This same increase was seen in the SbIII resistant line and to a much lesser extent in the miltefosine resistant line (Supplementary Table 1). This intracellular lipid relates to a formate (CH₂O₂) adduct of miltefosine and is therefore unlikely to be parasite derived, but instead derives from the drug itself, confirming the uptake of miltefosine. No metabolites could be found that would relate to a parasite-derived processing of miltefosine and the drug itself was unaltered from thin layer chromatography analysis (data not shown).

The altered metabolite profiles do not reveal an obvious primary metabolic target of miltefosine. This may mean that the initial target of miltefosine is not metabolic or that the metabolites affected by the target inhibition were not well ionised using this method.

3.2. The mode of action of miltefosine involves internal lipid remodelling

It was immediately evident that at the final 5 h time point in the wild-type cell line treated with miltefosine, many metabolites that

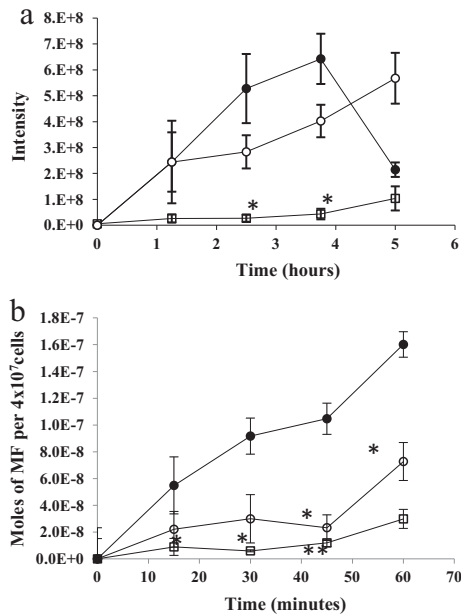


Fig. 2. Miltefosine uptake in JPCM5 wild-type and resistant promastigotes. Miltefosine accumulation measured by (a) mass spectrometry over 5 h and (b) by fluorescence (calculated as moles by comparing fluorescence levels to a standard curve) over 1 h. JPCM5 wild-type (●), MF200 (□) and SbIII2000.2 (○). An average of at least three independent biological replicates is shown, with error bars depicting the standard error of the mean. Stars indicate significance at $p < 0.05$ (*) or $p < 0.001$ (**).

had been stable throughout the time course displayed a sharp reduction in abundance (Supplementary Table 1). The cells appeared slightly smaller and more spherical after 5 h in drug (Fig. 1d), but the cell volume was not systematically measured. The drop in metabolite abundance could be due to a decrease in cell size but is much more likely to be due to cell leakage. We chose to analyse which metabolites were altered at the penultimate, 3.75 h time point, as the majority of metabolites (90%) were stable until this time point, indicating that the cell volume was not significantly altered. There was also no alteration in the membrane composition at this time point and no increase in lyso-phospholipids (all indicative that the membrane was not compromised). The growth curves corroborate this point (Fig. 1b).

There were 87 metabolites having a p value of <0.05 from a Student's t -test and a fold change of >2 at the penultimate time point in the wild-type cell line (Supplementary Table 3). Some of these metabolites did not show an obvious upwards or downwards trend and seemed to be very variable between the time points, but there was an upwards trend in many alkane fragments, which may be related to lipid metabolism (Fig. 3a). These metabolites were small saturated alcohols and carboxylates on alkane chains of between four and 10 carbons. Ethanolamine phosphate and putative 5-aminopentanoate were the only metabolites in this group to decrease over the time course. Metabolites related to sugars and bases also showed changes in abundance with a marked increase in putative glucosamine phosphate (Fig. 3b). The increase in putative glucosamine phosphate and the lipids are consistent with an increased lipid turnover, which would release alkane fragments and sugar amines. Miltefosine induces ROS at this penultimate time point in the wild-type cells (Fig. 1c) and ROS have been known to attack native membrane phospholipids. However, a lipidomic analysis of phospholipids did not reveal any significant changes after 3.75 h of miltefosine treatment (Fig. 4), only the uptake of unmetabolised miltefosine (data not shown).

Not all sugars showed an increase in abundance and some, such as D-glucose 6-phosphate, D-mannanate, 2-deoxy-L-arabinose and

1-deoxy-D-xylose showed a decreasing trend. It is difficult to conclusively identify five and six carbon sugars after separation by the ZIC-HILIC column, as these species have many stereoisomers, which do not separate efficiently and therefore have the same exact mass and very similar retention times.

The changes in internal lipid fragments (Fig. 3a), sugars (Fig. 3b), DNA, thiols, peptides (Fig. 3c) and others (Fig. 3d) observed in the wild-type cells were not observed in the MF200 line (Fig. 3, right insets). The SbIII resistant line, however, showed many of the same changes as the wild-type cells in terms of increased alkane fragments (Fig. 3a left inset), although to a lesser extent and without the metabolite leakage at 5 h. The sugars, DNA fragments, thiols, peptides and others (Fig. 3b–d, left insets) did not show such marked changes as in the wild-type line.

3.3. Evidence of cell stresses

ROS have previously been shown to attack DNA, causing DNA laddering (Moreira et al., 2011), which could result in the release of nucleotide fragments as seen in Fig. 3c. The release of nucleases may also be responsible for these fragments if the mitochondrial outer membrane was compromised. Some putative dipeptides are seen to increase in abundance (Fig. 3d), which could be a result of protein breakdown, but as there are only two dipeptide species represented, this seems unlikely. Putative trypanothione disulphide decreases slightly in abundance over the time course (Fig. 3d), whereas putative glutathione disulphide levels decrease at the 1.25 h time point before recovering and increasing significantly towards the 3.75 h time point (Supplementary Table 1). Trypanothione disulphide is a dithiol-polyamine constructed using two glutathione molecules conjugated via a spermidine linker (Fairlamb et al., 1985). The decrease in trypanothione may result from the release of glutathione to compensate for the shock decrease at the first time point. The spermidine peak was automatically rejected by the IDEOM software in this dataset because the ion was detected with a shoulder peak (two overlapping peaks with the same mass), but the spermidine standard run before the dataset confirms that this peak is in fact spermidine. The levels of spermidine appeared to show an initial decrease followed by a recovery (Supplementary Table 1, "rejected" tab), therefore if trypanothione is recycled to produce more glutathione, then the released spermidine must also be used for another purpose as spermidine's levels are not in accordance with those for glutathione. Unfortunately, the oxidation state of glutathione and trypanothione cannot be ascertained in this experiment as the method used results in the oxidation of these thiols. Ovothiol A and Ovothiol A disulphide, two other important thiols, fluctuated over the time course. Thiamin monophosphate also has a sulphur group and was significantly increased during miltefosine treatment (Fig. 3d). These cell stresses were not seen by either of the resistant lines (Fig. 3, insets), except for the decrease in trypanothione disulphide seen in the SbIII resistant line (to 59% after 5 h), which is similar to the decrease in wild-type cells (to 50% after 5 h) (Fig. 3d and Supplementary Table 3).

4. Discussion

Metabolomics studies are rare in parasitic protozoa, but have huge potential use to determine the MOA of the often very old and toxic drugs. A knowledge of the MOA of a compound is paramount to rational drug design to improve efficacy and to predict and reduce toxicity. Mechanisms of resistance to the compound can also be predicted if the MOA is known and synergistic compounds can be found that would reduce the chances of resistance developing.

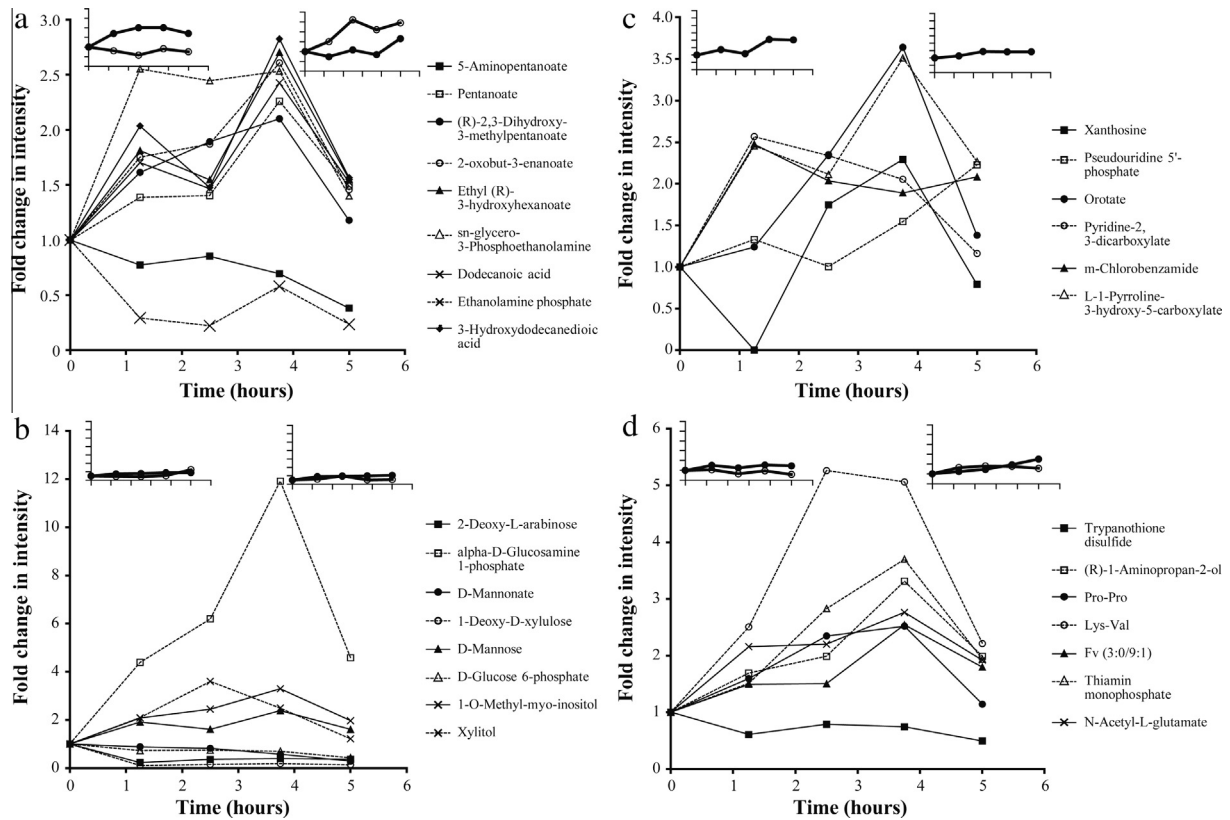


Fig. 3. Changes in the intensity of metabolites associated with miltefosine action. Metabolite changes in the wild-type line are sorted into groups for (a) alkane fragments, (b) sugars, (c) DNA fragments, thiols and peptides and (d) others. Inset graphs show average ratio changes in the SbIII2000.2 (top left) or MF200 (top right). To determine whether the metabolites that showed an upwards trend in the wild-type line also showed an upwards trend in the resistant lines an average of all the metabolites that increased in wild-type was taken for each resistant line. The same was done for metabolites that showed a downward trend in the wild-type line. (●) In inset graphs shows the average ratio of metabolites that increased in wild-type cells for each metabolite grouping. (○) In inset graphs shows the average ratio of metabolites that decreased in the wild-type cells. The scales are conserved in the inset graphs. An average of three replicates is shown and relative standard deviation for each point was below 0.5.

The MOA of miltefosine is undetermined, but there are three schools of thought in circulation: Akt inhibition leading to apoptosis, modulation of macrophage responses and changes to membrane phospholipid architecture. Here we show changes in the internal metabolome of *Leishmania* promastigotes over time in response to the xenobiotic miltefosine using LC-MS. We were also able to show accumulation of miltefosine in the wild-type cell line and show that the drug is not accumulated in the MF200 miltefosine resistant cell line. This was confirmed biochemically and SNPs were detected in the transporter for miltefosine that may cause this reduction in miltefosine accumulation. We were surprised to see a reduction in miltefosine accumulation in the Sb2000.2 mutant during the first 60 min (Fig. 2b) and even more surprised by the presence of SNPs in the MT gene for the SbIII2000.2 mutant. Sequencing of the MT gene in other antimony resistant mutants suggests that this is a rare event, but nevertheless the demonstration that MT can be mutated in an antimony resistant mutant opens the possibility for multidrug resistance.

Miltefosine treatment of wild-type promastigotes alters approximately 10% of the metabolome after 3.75 h, with many of the changes relating to an increase in short alkanes and sugars. The changes seen are synchronised with the production of reactive oxygen species. Membrane-incorporated lipids were not significantly altered in our experiments. This contradicts earlier research (Rakotomanga et al., 2004, 2007), but since the earlier published work was done with a lower drug concentration and for a longer period of time, their work may actually have been showing an adaptive response to miltefosine (Rakotomanga et al., 2007). Signs of DNA damage were also detected as were changes to the levels of

some thiols and polyamines (Fig. 3). Exogenous spermidine has previously been shown to increase the life span of yeast, nematodes, flies and human immune cells in culture (Eisenberg et al., 2009). The mechanism for this spermidine-induced death delay is not known, but it has been suggested that it may involve remodelling of chromatin and upregulation of autophagy, increasing resistance to oxidative stress (Eisenberg et al., 2009). When spermidine levels in *Trypanosoma cruzi*, a related kinetoplastid, are reduced, lipid peroxidation was shown to be increased. Spermine, a related polyamine not found in *Leishmania* (due to the lack of a spermine synthase) has also been observed to be effective at lipid peroxidation rescue (Hernández et al., 2006). The putative early release of spermidine (Supplementary Table 1) may help the cell to deal with miltefosine exposure.

After 5 h of miltefosine treatment on wild-type cells, there were depleted levels of most metabolites, which would indicate that the cells' outer membrane integrity had become compromised and metabolites were escaping during cell death. This may be due to the release of lipases following mitochondrial stress. The miltefosine resistant line did not accumulate miltefosine at all, did not display a ROS induction and did not show the alterations to the lipids, sugars and nucleobases that the wild-type line did.

It must be noted that all studies of miltefosine mode of action to date have been performed on promastigote cells so caution must be taken when applying the results to the parasite in general. However, metabolomic studies on intracellular parasites are problematic due to the generic nature of the measured metabolites and the inability to determine whether they are parasite or host derived. These data suggest that the mode of action of miltefosine

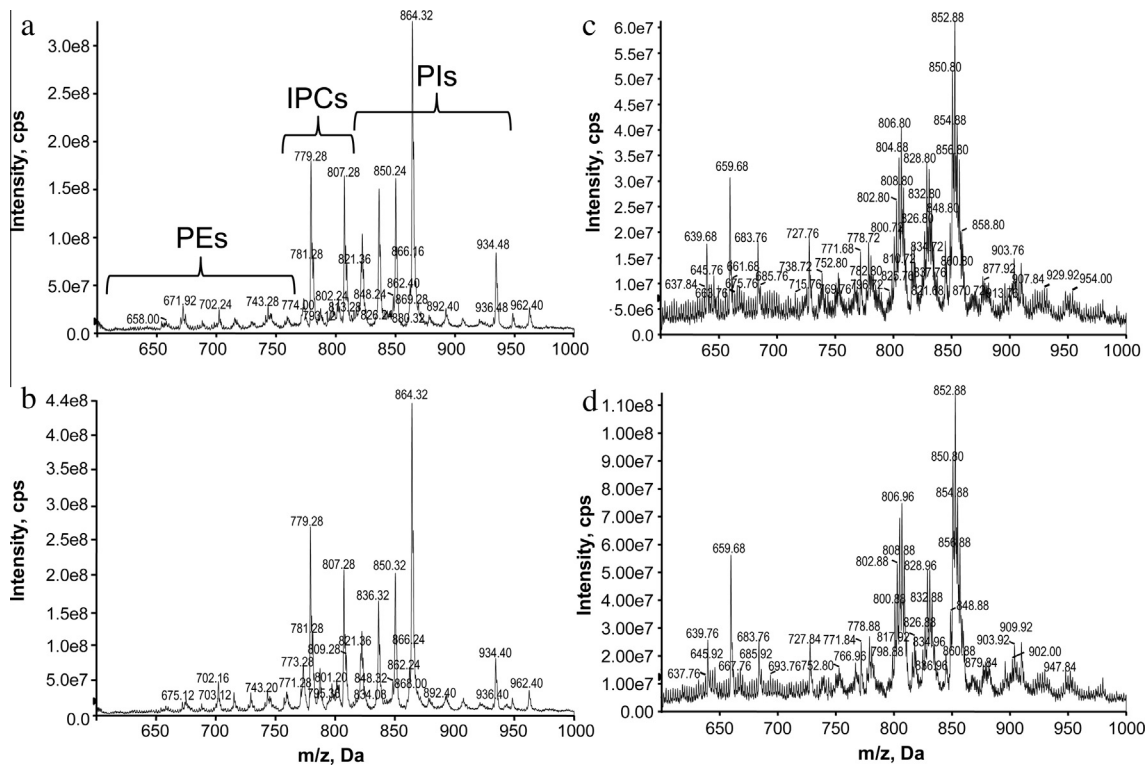


Fig. 4. There are no significant changes to the membrane lipids after miltefosine treatment. Negative ion ES-MS survey scans (600–1000 m/z) of total lipid extracts from *L. infantum* in the (a) absence or (b) presence of miltefosine (20.6 μM) for 3.75 h. Positive ion ES-MS survey scans (600–1000 m/z) of total lipid extracts from *L. infantum* in the (c) absence or (d) presence of miltefosine for 3.75 h. PEs: phosphoethanolamines, IPCs: inositol phosphocholines and PIs: phosphoinositols. An example of one of three independent biological replicates (which showed similar profiles) is shown.

in promastigote *Leishmania* is due to cell lysis preceded by alterations to internal lipid metabolism causing increases in alkanes, sugars and nucleotides. These alterations probably occur through the induction of reactive oxygen species. Understanding the mode of action of miltefosine is useful to help to develop effective combination therapies to ensure that resistance to any of the drugs is much less likely. Combining miltefosine with a drug that depreciates the cell's capacity to deal with ROS, such as the polyamine pathway inhibitor, eflornithine, is likely to be synergistic and could be considered for therapeutic use.

Conflicts of interest

The authors declare no conflicts of interest.

Acknowledgements

M.O. is a Canada research chair in antimicrobial resistance. This work was funded by the Canadian Institutes of Health Research (Grant number 13233). The Polyomics facility at the University of Glasgow is funded by The Wellcome Trust and the Scottish Universities Life Science Alliance. L.R. is funded by Ministerio de Economía y Competitividad (FIS PI 12-02706). T.K.S. is supported by a Wellcome Trust Grant 093228.

Appendix A. Supplementary data

Supplementary data associated with this article can be found, in the online version, at <http://dx.doi.org/10.1016/j.ijpddr.2013.11.002>.

References

- Bligh, E.G., Dyer, W.J.A., 1959. Rapid method of total lipid extraction and purification. *Can. J. Biochem. Physiol.* 37 (8), 911–917.
- Choudhury, K., Zandera, D., Kube, M., Reinhardt, R., Clos, J., 2008. Identification of a *Leishmania infantum* gene mediating resistance to miltefosine and SbIII. *Int. J. Parasitol.* 38 (12), 1411–1423.
- Coelho, A.C., Boisvert, S., Mukherjee, A., Leprohon, P., Corbeil, J., Ouellette, M., 2012. Multiple mutations in heterogeneous miltefosine-resistant *Leishmania major* population as determined by whole genome sequencing. *PLoS Negl. Trop. Dis.* 6 (2), e1512.
- Creek, D.J., Jankevics, A., Burgess, K.E., Breitling, R., Barrett, M.P., 2012. IDEOM: an Excel interface for analysis of LC-MS-based metabolomics data. *Bioinformatics* 28 (7), 1048–1049.
- Croft, S.L., Sundar, S., Fairlamb, A.H., 2006. Drug resistance in leishmaniasis. *Clin. Microbiol. Rev.* 19 (1), 111–126.
- Dorlo, T.P., Balasegaram, M., Beijnen, J.H., de Vries, P.J., 2012. Miltefosine: a review of its pharmacology and therapeutic efficacy in the treatment of leishmaniasis. *J. Antimicrob. Chemother.* 67, 2576–2597.
- Eisenberg, T., Knauer, H., Schauer, A., Büttner, S., Ruckstuhl, C., Carmona-Gutierrez, D., Ring, J., Schroeder, S., Magnes, C., Antonacci, L., Fussi, H., Deszcz, L., Hartl, R., Schraml, E., Criollo, A., Megalou, E., Weiskopf, D., Laun, P., Heeren, G., Breitenbach, M., Grubeck-Loebenstein, B., Herker, E., Fahrenkrog, B., Fröhlich, K.U., Sinner, F., Tavernarakis, N., Minois, N., Kroemer, G., Madeo, F., 2009. Induction of autophagy by spermidine promotes longevity. *Nat. Cell Biol.* 11 (11), 1305–1314.
- Fairlamb, A.H., Blackburn, P., Ulrich, P., Chait, B.T., Cerami, A., 1985. Trypanothione: a novel bis(glutathionyl)spermidine cofactor for glutathione reductase in trypanosomatids. *Science* 227 (4693), 1485–1487.
- Getachew, F., Gedamu, L., 2012. *Leishmania donovani* mitochondrial iron superoxide dismutase A is released into the cytosol during miltefosine induced programmed cell death. *Mol. Biochem. Parasitol.* 183 (1), 42–51.
- Hernández, S.M., Sánchez, M.S., de Tarlovsky, M.N., 2006. Polyamines as a defense mechanism against lipoperoxidation in *Trypanosoma cruzi*. *Acta Trop.* 98 (1), 94–102.
- Hornillos, V., Carrillo, E., Rivas, L., Amat-Guerri, F., Acuña, A.U., 2008. Synthesis of BODIPY-labeled alkylphosphocholines with leishmanicidal activity, as fluorescent analogues of miltefosine. *Bioorg. Med. Chem. Lett.* 18 (24), 6336–6339.
- Imbert, L., Ramos, R.G., Libong, D., Abreu, S., Loiseau, P.M., Chaminade, P., 2012. Identification of phospholipid species affected by miltefosine action in

- Leishmania donovani* cultures using LC-ELSD, LC-ESI/MS, and multivariate data analysis. *Anal. Bioanal. Chem.* 402 (3), 1169–1182.
- Lux, H., Hart, D.T., Parker, P.J., Klenner, T., 1996. Ether lipid metabolism, GPI anchor biosynthesis, and signal transduction are putative targets for anti-leishmanial alkyl phospholipid analogues. *Adv. Exp. Med. Biol.* 416, 201–211.
- Moreira, W., Leprohon, P., Ouellette, M., 2011. Tolerance to drug-induced cell death favours the acquisition of multidrug resistance in *Leishmania*. *Cell Death Dis.* 2, e201.
- Pérez-Victoria, F.J., Castanys, S., Gamarro, F., 2003a. *Leishmania donovani* resistance to miltefosine involves a defective inward translocation of the drug. *Antimicrob. Agents Chemother.* 47 (8), 2397–2403.
- Pérez-Victoria, F.J., Gamarro, F., Ouellette, M., Castanys, S., 2003b. Functional cloning of the miltefosine transporter. A novel P-type phospholipid translocase from *Leishmania* involved in drug resistance. *J. Biol. Chem.* 278 (50), 49965–49971.
- Pérez-Victoria, J.M., Cortés-Selva, F., Parodi-Talice, A., Bavchvarov, B.I., Pérez-Victoria, F.J., Muñoz-Martínez, F., Maitrejean, M., Costi, M.P., Barron, D., Di Pietro, A., Castanys, S., Gamarro, F., 2006a. Combination of suboptimal doses of inhibitors targeting different domains of LtrMDR1 efficiently overcomes resistance of *Leishmania* spp. to miltefosine by inhibiting drug efflux. *Antimicrob. Agents Chemother.* 50 (9), 3102–3110.
- Pérez-Victoria, F.J., Sánchez-Cañete, M.P., Castanys, S., Gamarro, F., 2006b. Phospholipid translocation and miltefosine potency require both *L. donovani* miltefosine transporter and the new protein LdRos3 in *Leishmania* parasites. *J. Biol. Chem.* 281 (33), 23766–23775.
- Proto, W.R., Coombs, G.H., Mottram, J.C., 2013. Cell death in parasitic protozoa: regulated or incidental? *Nat. Rev. Microbiol.* 11 (1), 58–66.
- Rakotomanga, M., Loiseau, P.M., Saint-Pierre-Chazalet, M., 2004. Hexadecylphosphocholine interaction with lipid monolayers. *Biochim. Biophys. Acta* 1661 (2), 212–218.
- Rakotomanga, M., Blanc, S., Gaudin, K., Chaminade, P., Loiseau, P.M., 2007. Miltefosine affects lipid metabolism in *Leishmania donovani* promastigotes. *Antimicrob. Agents Chemother.* 51 (4), 1425–1430.
- Richmond, G.S., Gibellini, F., Young, S.A., Major, L., Denton, H., Lilley, A., Smith, T.K., 2010. Lipidomic Analysis of bloodstream and procyclic form *Trypanosoma brucei*. *Parasitology* 137 (9), 1357–1392.
- Ruiter, G.A., Zerp, S.F., Bartelink, H., van Blitterswijk, W.J., Verheij, M., 2003. Anti-cancer alkyl-lysophospholipids inhibit the phosphatidylinositol 3-kinase-Akt/PKB survival pathway. *Anticancer Drugs* 14 (2), 167–173.
- Scheltema, R.A., Jankevics, A., Jansen, R.C., Swertz, M.A., Breitling, R., 2011. PeakML/mzMatch: a file format, Java library, R library, and tool-chain for mass spectrometry data analysis. *Anal. Chem.* 83 (7), 2786–2793.
- Seiferta, K., Pérez-Victoria, F.J., Stettler, M., Sánchez-Cañete, M.P., Castanys, S., Gamarro, F., Croft, S.L., 2007. Inactivation of the miltefosine transporter, LdMT, causes miltefosine resistance that is conferred to the amastigote stage of *Leishmania donovani* and persists *in vivo*. *Int. J. Antimicrob. Agents* 30 (3), 229–235.
- Vincent, I.M., Creek, D.J., Burgess, K., Woods, D.J., Burchmore, R.J., Barrett, M.P., 2012. Untargeted metabolomics reveals a lack of synergy between nifurtimox and eflornithine against *Trypanosoma brucei*. *PLoS Negl. Trop. Dis.* 6 (5), e1618.
- WHO, 2010. Working to overcome the global impact of neglected tropical diseases. First WHO report on neglected tropical diseases, WHO, Geneva.
- Williams, R.A.M., Smith, T.K., Cull, B., Mottram, J.C., Coombs, G.H., 2012. ATG5 is essential for autophagy and mitochondrial homeostasis in *Leishmania*. *PLoS Pathog.* 8 (5), e1002695.
- Zufferey, R., Mamoun, C.B., 2002. Choline Transport in *Leishmania major* promastigotes and its inhibition by choline and phosphocholine analogs. *Mol. Biochem. Parasitol.* 125, 127–134.